3D Printing of Cellulose Nanocrystal-Loaded Hydrogels through Rapid Fixation by Photopolymerization

3D printing of cellulose nanocrystals-loaded hydrogels through rapid fixation by photopolymerization

Journal:	*Langmuir*
Manuscript ID	la-2021-00553j
Manuscript Type:	Article
Date Submitted by the Author:	25-Feb-2021
Complete List of Authors:	Kam, Doron; Robert H Smith Institute of Plant Sciences and Genetics in Agriculture; Hebrew University of Jerusalem, Casali Institute of Applied Chemistry Braner, Ariel; Hebrew University of Jerusalem, Casali Institute of Applied Chemistry; Future scientist center, Alpha program Abouzglo, Avi; Hebrew University of Jerusalem, Casali Institute of Applied Chemistry Larush, Liraz; Hebrew University of Jerusalem, Casali Institute of Applied Chemistry Chiappone, Annalisa; Politecnico di Torino, DISAT Shoseyov, Oded; Robert H Smith Institute of Plant Sciences and Genetics in Agriculture Magdassi, Shlomo; Hebrew University of Jerusalem, Casali Institute of Applied Chemistry

3D printing of cellulose nanocrystals-loaded hydrogels through rapid fixation by photopolymerization

Doron Kam[12], Ariel Braner[13], Avi Abouzglo[1], Liraz Larush[1], Annalisa Chiapponed[4], Oded Shoseyov[2], Shlomo Magdassi[1]**

[1]Institute of Chemistry, The Hebrew University of Jerusalem, Jerusalem, Israel

[2]Plant Sciences and Genetics in Agriculture, The Hebrew University of Jerusalem, Rehovot, Israel

[3]Alpha program, Future scientist center, Jerusalem, Israel

[4]Department of Applied Science and Technology, Politecnico di Torino, Torino, Italy.

ABSTRACT

New ink compositions for direct ink writing (DIW) printing of hydrogels, combining the superior rheological properties of cellulose nanocrystals (CNC) and a novel water-compatible photoinitiator, are presented. Rapid fixation was achieved by photopolymerization induced immediately after printing of each layer by 365 nm light for 5 s, which overcame the common height limitation in DIW printing of hydrogels, and enabled the fabrication of objects with a high-aspect ratio. CNC imparted a unique rheological behavior, which manifested by orders of magnitude difference in viscosity between low and high shear rates, and in rapid high-shear recovery, without compromising ink printability. Compared to the literature, the presented printing compositions enable the use of low photoinitiator concentrations under the shortest curing time and are also curable by 405nm, which is favorable for maintaining viability in bio-inks.

Keywords: 3D printing; nanocellulose; hydrogel; water-compatible photoinitiator

INTRODUCTION

3D printing, also known as additive manufacturing, has become an important fabrication technology during the past decade, and is already implemented in a variety of fields, such as automotives [1], aerospace [2], dentistry [3], soft robotics [4], and even pharmaceutics.[5] In particular, 3D bioprinting, which addresses current challenges in medicine, such as bone scaffold and even printed heart mimics composed of hydrogels, is an emerging and continuously evolving field.[6–8] The most common 3D bioprinting technology for printing hydrogel is based on extrusion, also known as direct ink writing (DIW), which forms objects by extruding successive layers of materials, layer after layer, along a predesigned pathway. Other hydrogel-based printing techniques such as vat photopolymerization,[9] and material jetting systems,[10] yield high resolution far beyond that needed for biological purposes. In addition, when using these techniques, the cell composition of the tissue/organ and the bioinks are currently a major obstacle due to clogging of nozzles by the cells or the lack of vat multi-material printing technology. Therefore, despite of the limited resolution of extrusion-based printing as compared to vat polymerization and material jetting, it is plausible that it will remain as the preferred technology for bioprinting clinically relevant constructs.[11]

3D printing through extrusion-based technologies requires (1) sufficient ink viscosity to maintain it in the extruder, (2) ink flow, achieved by applying pressure during the extrusion, (3) shape fidelity, achieved by retaining high viscosity upon contact with the printer platform, and (4) rapid fixation to prevent the collapse of the printed structure.

Shape fidelity in DIW is very challenging, due to conflicting ink specifications, which are governed by ink rheology properties that tackle gravity and surface energy. When the printed material does not undergo a rapid fixation process, the printed object can slump after exceeding a

certain height due to gravity, a height that is determined by the rheological ink properties. For example, for 45 wt% Boehmite suspension, slumping occurs already at a height of 5 mm.[12] To obtain greater heights, the ink yield stress must be increased, however, this interferes with the printability of the ink. Alternatively, high objects can be fabricated by inducing an immediate increase in viscosity of the printed structure during the printing process via a photopolymerization reaction, as performed in inkjet printing by the Polyjet technology.[13] Inkjet printing requires inks with very low viscosities, which are not suitable for printing high-viscosity polymer solutions.

DIW combined with UV photopolymerization, has been used to print hydrogels composed of gelatin methacryloyl.[14,15] The printing compositions contained the photoinitiator (PI) Irgacure 2959, which is water-soluble, but has very low absorption in the wavelengths which are relevant to current 3D printers (365-405nm).[16] Thus, to achieve rapid and efficient photopolymerization, there is a need for a water-soluble PI that absorbs well at the relevant wavelengths. Therefore, here we utilize our recently reported water-compatible PI 2,4,6-trimethylbenzoyl-diphenylphosphine oxide (TPO), which by itself is not soluble in water. TPO is suitable for photopolymerization at 405 nm, which is favorable for bioprinting and cell viability. Rapid fixation to obtain high-aspect ratio objects can not be achieved by photopolymerization alone due to time-lapse between the point of extrusion and the point at which the ink meets the light irradiation. Therefore, we used a dual-fixation mechanism, based on both polymerization and rheology. The latter can be achieved using cellulose nanocrystals (CNCs) which is a biocompatible material that had shown to be favorable for DIW.[17,18]

CNCs are nanometric rod particles, which originate from cellulose hydrolysis mainly by sulfuric acid.[19,20] CNC integration in photopolymerizable hydrogels was mainly achieved by its chemical or physical entrapment within a hydrated polymer network.[21] Chemical modification of CNC by

polymerizable groups, such as acrylates and methacrylates, may impair its water dispersibility and therefore, the water medium should be replaced by solvents.[22,23] poly(N,N-dimethacrylamide) (PDMA) hydrogels were reinforced by acrylated CNCs dispersed in water in the presence of 2,2'-diethoxyacetophenone (Irgacure 2959), the most common water-soluble PI at that time. However, the polymerization reaction required 50 min, which is a too long time for rapid fixation in DIW processes.[24]

A previous work on physical entrapment of CNCs demonstrated hydrogel fabrication in molds with inks containing CNC with various monomers. 2,2-diethoxyacetophenone was used as a photo-initiator, in a photo-polymerization process that was carried out for 1 hour.[25] Later, the same group used different PIs and UV polymerized the ink for 3 hours.[26] Zhang et al. used DMSO as the liquid medium for DIW, and Irgacure 2959, applied UV irradiation for 10 min.[27] Frost et al. used lithium phenyl-2,4,6-trimethylbenzoylphosphinate (LAP) as a water-soluble PI for DIW printing and reported on polymerization within 60 s in UV post-curing chamber.[28] There are also some reports on the application of inks containing CNC in vat printing processes, in which the photopolymerization is faster than in DIW but occurs within a thinner layer of ink, in the micron-size range.[29–31]

Figure 1 summarizes the literature data regarding the photopolymerization-based fabrication of 3D hydrogel objects including CNC, emphasizing the long duration required to achieve photopolymerization of hydrogels and the high concentration of PI that is needed; due to the high water content in typical hydrogels, their reactivity is usually low, thus requiring light exposure times that are too long for practical purposes.

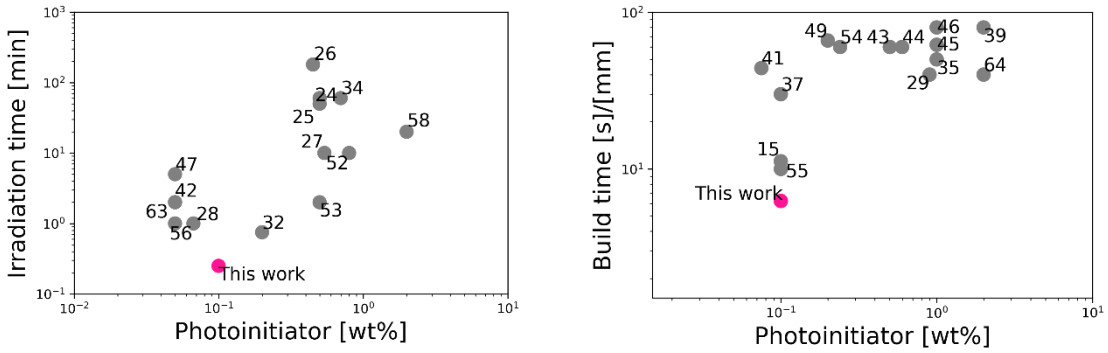

(A) (B)

Figure 1. Summary of photocurable hydrogels. PI concentration based on (A) One-time illumination (mold or post-curing) (B) build time (various 3D printing technique). See supporting information Table S1-2.[14,15,22–63]

Here, we present new hydrogel compositions for DIW printing, which utilizes the unique pseudoplastic behavior of CNC, combined with rapid fixation of the printed objects by photopolymerization. The developed formulations composed of CNC and water-compatible PIs enable the unprecedented reduction of exposure times, down to approximately 5 s, which results in the most rapid buildup rate (Fig 1). By using the proposed ink compositions, hydrogels with high-aspect ratio, excellent shape fidelity, and superior mechanical properties can be achieved in a rapid printing process.

MATERIALS AND METHODS

Materials. Cellulose nanocrystal (CNC) dispersions were obtained from Celluforce Inc., Montreal, Canada (freeze-dry, LOT #2015-009). Acrylic acid (AA), isopropanol (IPA) and Brij 58 were purchased from Sigma-Aldrich. Polyethyleneglycol diacrylate (PEGDA) (SR610) was obtained from SARTOMER. 2,4,6-trimethylbenzoyl-diphenylphosphine oxide (TPO) PI was obtained from IGM.

Water-compatible PI. A water-compatible powder composed of 5 wt% 2,4,6-trimethylbenzoyl-diphenylphosphine oxide (TPO) PI and 95 wt% Brij58 was prepared based on previous publications.[37,54] Upon addition 1 wt% to water or the hydrogel ink composition, it forms a clear solution.

Ink preparation . A 10 wt% dispersion of CNC in TDW was prepared by sonication (Vibra-Cell, Sonics & Materials) (750W, 15 min, pulses of 2 s on, 1 s pause) in an ice water bath to prevent overheating. The obtained dispersion was mixed with the other materials as indicated in **Table 1**, using a planetary mixer for 5 min, and was defoamed for 2 min (AR-100, THINKY Co. Ltd, Japan). The final ink compositions were kept in a 10 mL disposable syringe without exposure to light.

Table 1. Inks compositions

	0%CNC	1.2%CNC	2.4%CNC	3.6%CNC	5.8%CNC
10%CNC [g]	0	5	10	15	23.2
AA [g]	17.3	16.85	16.4	15.95	15.2
TDW [g]	23.2	18.2	13.2	8.2	0
PEGDA [g]	0.9	0.88	0.86	0.83	0.8
TPO-Brij [g]	0.9	0.88	0.86	0.83	0.8

Rheology. Rheology measurements were performed at room temperature (20 °C) using a HaakeRheostress 6000 Rheometer (Thermo Fisher Scientific, Waltham, MA, USA) coupled with an RS6000 temperature controller (lower plate - TMP 350, upper plate - P35TiL, gap - 0.5 mm). All experiments started at a constant low shear rate ($\dot{\gamma} = 0.01\frac{1}{s}$, t=100s, T=20 °C) to reach the set temperature and to achieve a defined shear history before the actual experiment. Then, for the viscosity-shear rate curves, the shear rate was ramped up from $\dot{\gamma} = 0.01\frac{1}{s}$ to $\dot{\gamma} = 100\frac{1}{s}$ at t=100

s. For thixotropic measurements, the shear was ramped up from $\dot{\gamma}$=0.01 1/s to $\dot{\gamma}$=100 1/s, then held at a maximum shear rate ($\dot{\gamma} = 100\frac{1}{s}$) for 30 s, and then ramped down to $0.1\frac{1}{s}$. For shear recovery measurements, a constant shear rate of $\dot{\gamma} = 0.1\frac{1}{s}$ was applied for 100s, followed by a high shear rate of $\dot{\gamma} = 100\frac{1}{s}$ for 30 s, and then a low shear rate $\dot{\gamma} = 0.1\frac{1}{s}$ for another 100s. An oscillation amplitude sweep was performed at frequencies 1 Hz and 10 Hz, over a stress range of $1\ Pa \leq \tau \leq 100\ Pa$. An oscillation frequency sweep was performed at 10 Pa Hz, over a frequency range of $0.01\ Hz \leq f \leq 100\ Hz$.

Photorheology. Photorheolgical measurements were performed at 25°C using an Anton PAAR Modular Compact Rheometer (Physica MCR 302) in parallel-plate mode, using a quartz bottom plate. A Hamamatsu LC8 lamp with a UV-light source (25 mWcm^{-2}) was placed under the bottom plate. Experiments were performed in flow mode, by setting the gap between the two glass plates to 0.3 mm. A constant shear rate of $\dot{\gamma}$=0.1 s^{-1} was imposed and the UV irradiation was started after 60 s to allow the system to stabilize. Viscosity change was monitored as a function of irradiation time.

Mechanical testing. Hydrogel objects for the evaluation of mechanical properties were fabricated in molds by exposing to 395 nm light (32V, 8A, Integration technology LTD, Oxon, UK) for 15 s. Unconfined mechanical tests of cylindrical objects were performed on fully swollen samples (over 72 h), using an Instron universal testing machine (Model 3345, Instron Corp., Norwood, MA, USA) equipped with a 500 N load cell and operated at 5 mm/min. Five replicate specimens were tested under ambient conditions. Young's modulus was calculated up to 15% strain, by linear least-squares regression (Scipy.stats.linregress).

3D printing. Hydrogels were 3D-printed using a Hyrel3D 30M printer (Hyrel International, Inc., Norcross, GA, USA) equipped with an SDS-10 extruder mounted with 365 nm LED. A 10

mL disposable syringe with a 16-gauge conical tip (1.29 mm) was used throughout the printing process unless indicated otherwise. G-code files were prepared via 3D Slic3r software (Ver. 1.2.9, slic3r.org). The printing rate was set to 5 mm/s, the layer height was set to 0.8 mm, and the light irradiation (365 nm or 405 nm) was applied for 5s for each printed layer.

Statistical analysis. All errors indicate 95% confidence interval (CI) and had been calculated by:

$$CI = \frac{f(t)\cdot\sigma}{\sqrt{N}},$$

where N is the sample size, $f(t)$ is the value of the Student's t-distribution for a specific probability (0.95) and $N-1$ degrees of freedom, and σ is the standard deviation.

RESULTS AND DISCUSSION

Our printing approach is based on combining the pseudoplastic behavior of the ink with rapid fixation of the printed layer. The CNC, which controls the rheological properties of the tested ink, enables obtaining a yield stress value that is sufficient for temporary fixation of a layer printed by extrusion. After each layer is formed, it is exposed to UV light, to initiate photopolymerization, which rapidly fixates the permanent shape of the layer. To achieve this, water-based UV-curable inks for DIW, composed of the monomers AA and PEGDA, and TPO as the PI, were prepared. As TPO is insoluble in water, we used our developed water-compatible TPO composition, with Brij-58, a nonionic surfactant.[37] Since the viscosity of this photocurable ink is not suitable for DIW printing, we supplemented it with dispersed CNC to tailor the rheological properties.

Five concentrations of CNC nanoparticles were prepared while maintaining the same concentration of solids in the ink (**Table 1**). Inks without CNC failed to print objects, as shown as a puddle, in Figure 2A. Additionally, objects printed with CNC-containing ink, but only exposed to UV irradiation after the objects were printed, failed to maintain their weight and shape beyond

a very small number of layers as seen in structure slumping (Figure 2B). The combination of CNC and UV curing during printing enabled the printing of objects with multiple highly stable layers (Figure 2C).

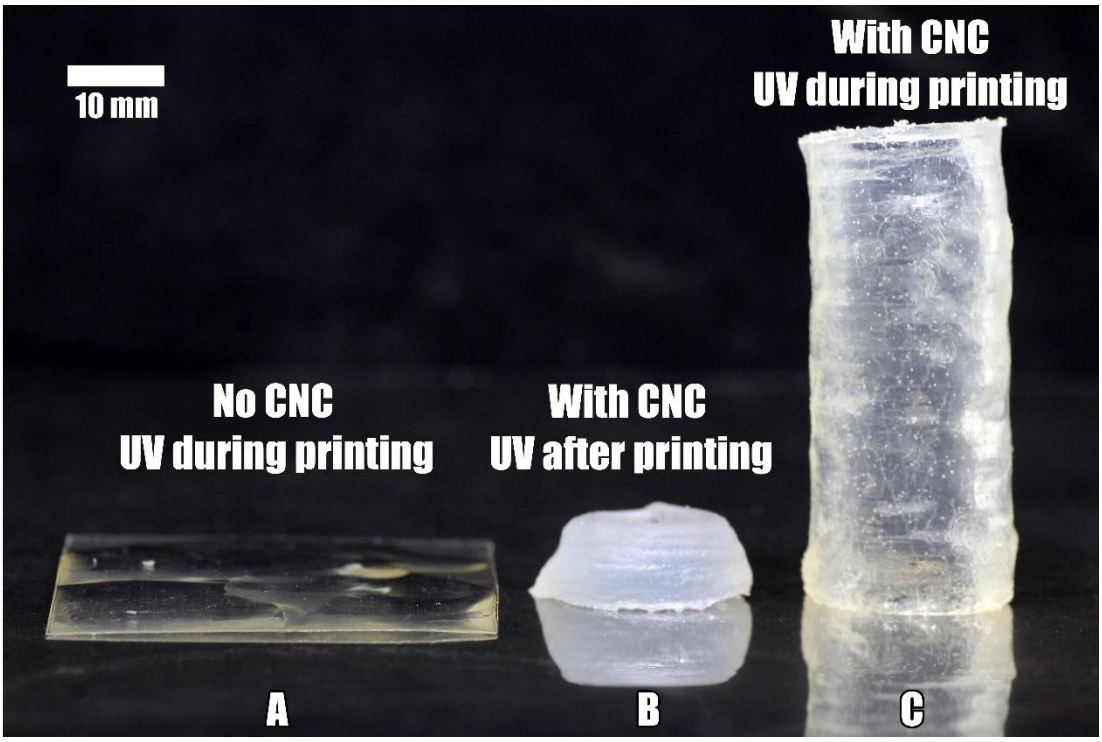

Figure 2. DIW-printed objects (A) with 0% CNC and UV-cured during printing (B) with 2.4% CNC and UV-cured after printing; the object is composed of 14 printed layers. (C) A cylindrical object printed with 2.4% CNC and UV-cured during printing. The object contains 32 printed layers.

Rheology. Rheology measurements were performed to examine ink behavior during the different steps of the printing process. First, flow curve experiments were performed, to determine how viscosity varies with shear rates. Sufficiently high viscosity at a low shear rate is crucial to avoid ink drippage from the syringe during non-printing steps, whereas when stress is applied by the syringe piston, viscosity must decrease rapidly to enable extrusion. As shown in **Figure** 3,

shear-thinning occurred only in samples that contained CNC. In addition, the viscosity increased as CNC concentrations increased, while shear-thinning behavior was preserved.

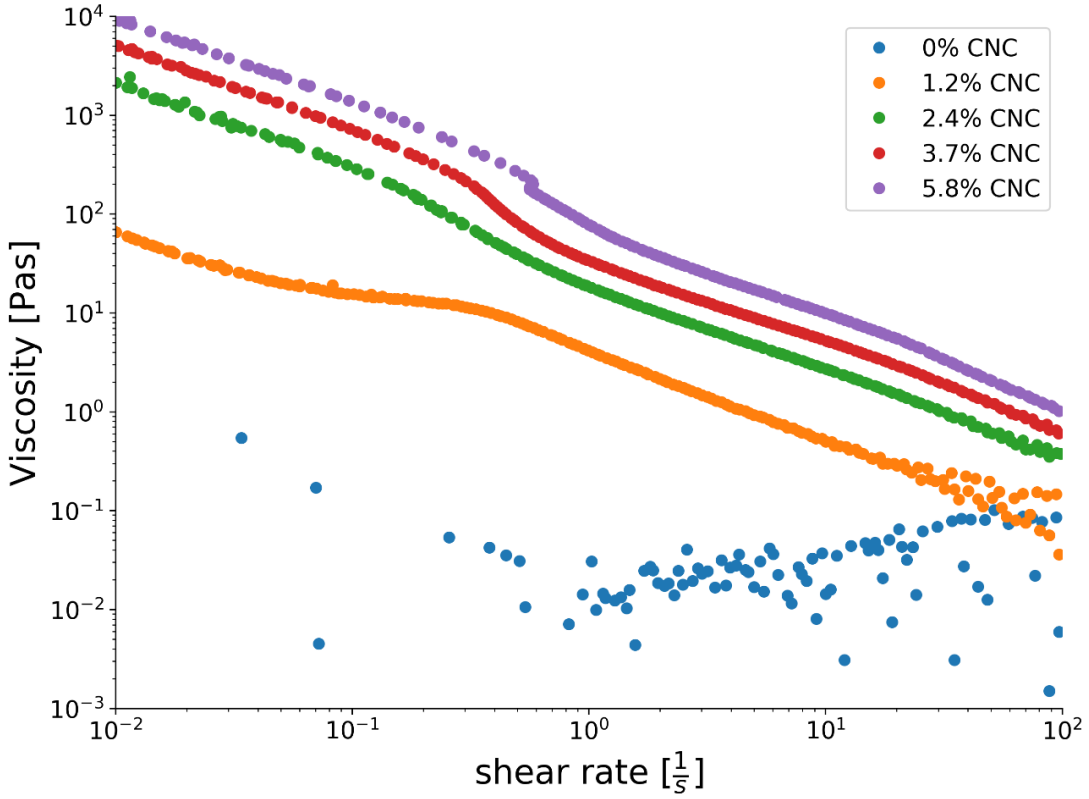

Figure 3. Viscosity as a function of shear rate for different CNC wt% hydrogel inks before exposure to UV light, plotted on a double logarithmic scale.

In addition to shear-thinning properties, inks used in extrusion-based 3D printers must be thixotropic, which enables them to return to their more viscous state, both in the syringe while not printing, and in the printed object, after being extruded. Thixotropy was evaluated by measuring viscosity at three stages: (1) when ramping up shear rate from $\dot{\gamma} = 0.1\frac{1}{s}$ to $\dot{\gamma} = 100\frac{1}{s}$, which causes a breakdown of ink structure, seen by the decrease in viscosity, (2) when holding a maximum shear rate for 30 s, and (3) when ramping down the shear rate to $\dot{\gamma} = 0.1\frac{1}{s}$ while the viscosity recovers by reforming the initial network within the ink. Figure 4A presents the

thixotropy behavior of CNC-containing inks. The thixotropy index, calculated from the area of the hysteresis loop from structure breakdown to recovery, represents the energy consumption of this process (**Figure** 4B). All inks containing CNC exhibited thixotropic behavior.

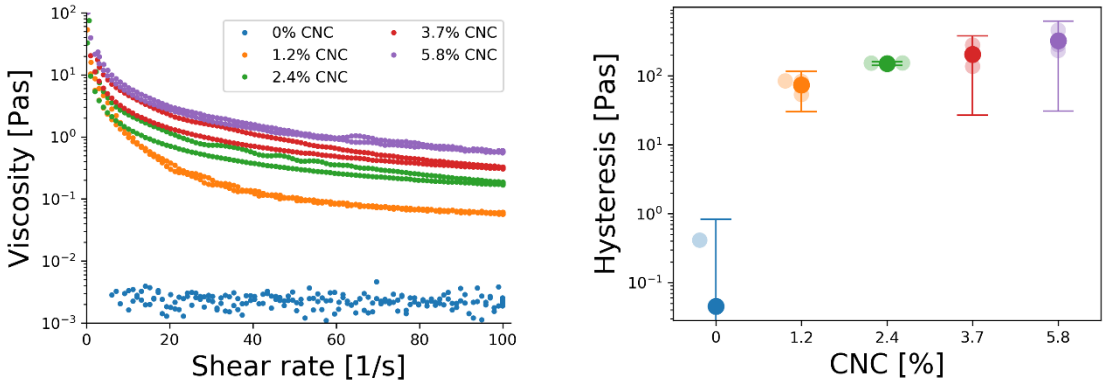

(A) (B)

Figure 4. Thixotropy measurement (A) Thixotropy viscosity hysteresis loop (B) Thixotropy index. Light-shaded markers represent actual measurement, dark-shaded markers represent average, and error bars indicate 95% CI.

Shear recovery experiments were performed to evaluate the rheology time dependence of the inks after extrusion. To correlate these measurements with the actual printing shear rate, the maximum shear rate (MSR) was evaluated. MSR of the printer setup was found to be between 75 1/s and 300 1/s, depending on the calculation, which takes into account the rheology dependence on CNC concentration (see supporting information section S2).

In this experiment (Figure 5), a constant low shear rate ($\dot{\gamma}$=0.1 1/s, T=20 °C) was applied for 100 s, followed by a constant high shear rate ($\dot{\gamma}$=100 1/s T=20 °C) for 30 s, simulating the shear rates which are applied from the syringe piston. Then, the shear rate was decreased again ($\dot{\gamma}$=0.1 1/s, T=20 °C) and the recovery of the viscosity was measured and compared to the initial viscosity. For all inks tested, a mean 5 s were required to recover 50% of the viscosity, after applying a shear

rate of 100 $^{1}/_{s}$. Moreover, it was noted that the higher the CNC concentration, the longer it took to reach a steady viscosity. The highest recovery (70.36%) was obtained with the ink containing 2.4% CNC, and was reached within 15 s.

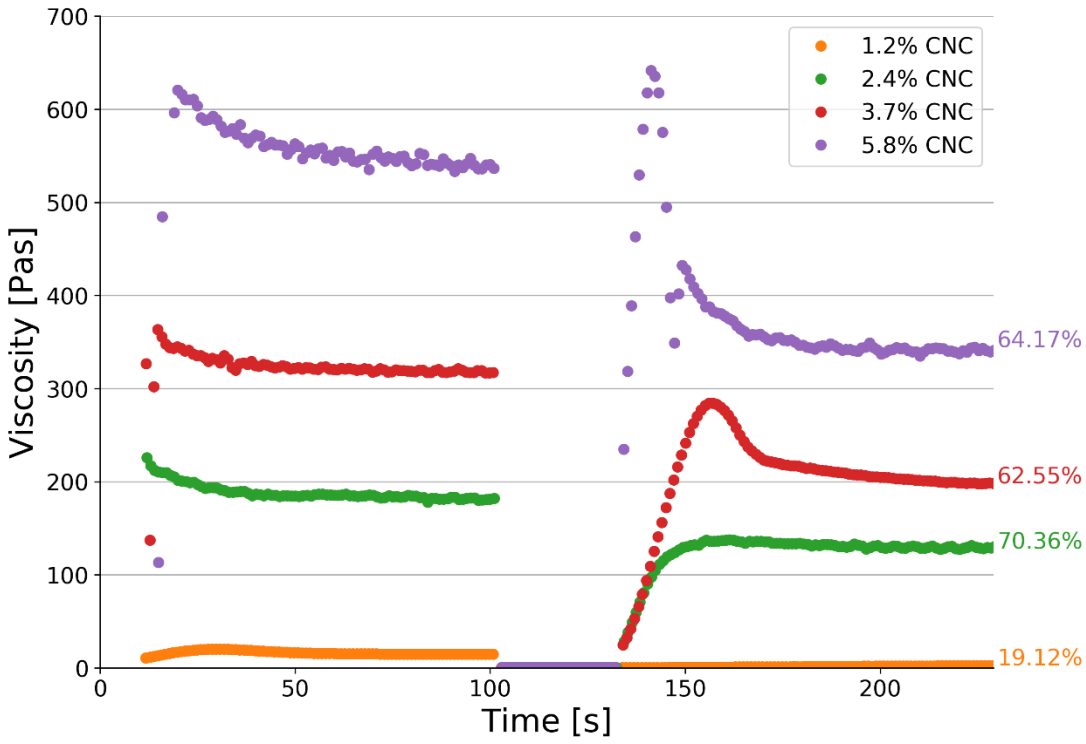

Figure 5. Shear recovery measurements at 100 $^{1}/_{s}$ shear rate. % recovery achieved is indicated shown to the right of each curve.

Mechanical properties of objects in mold. The mechanical properties of hydrogel objects fabricated, in molds, from inks containing various CNCs concentrations, were evaluated by unconfined compression tests (raw data is presented in Figure S2). As shown in **Figure** 6B, the Young's modulus increased with increasing CNC concentrations, with the best precision obtained for the 2.4% ink. The same trend was observed for the stress-at-break evaluations, which increased three-fold for ink ranging from 0% to 2.4% CNC wt%, without impacting precision (**Figure** 6D).

At higher CNC concentrations, the stress at break continued to increase, but the precision began to decrease. Interestingly, CNC concentration did not affect strain-to-break (**Figure** 6C).

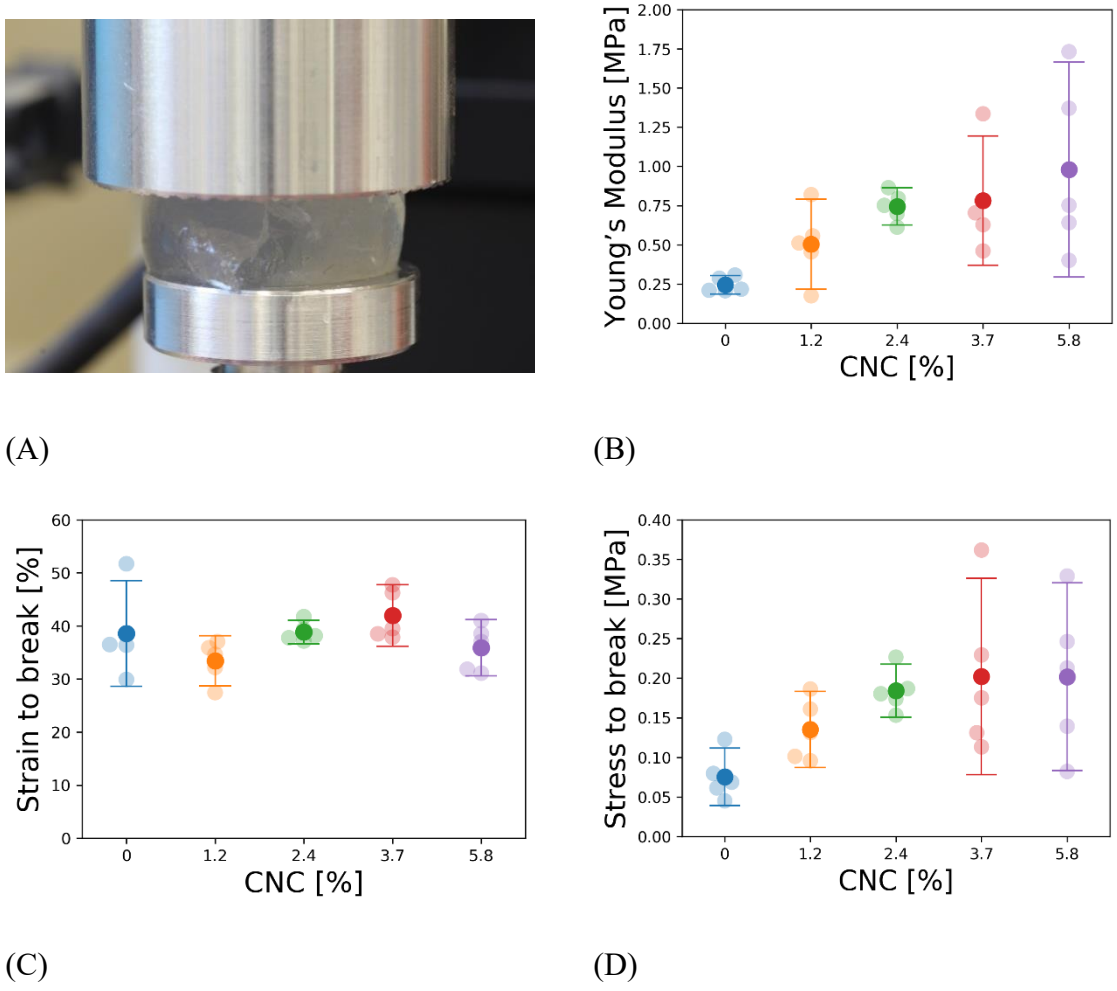

(A) (B)

(C) (D)

Figure 6. Unconfined compression test of hydrogels integrating various concentrations of CNC. (A) Image of hydrogel during the test. (B) Young's modulus. (C) Strain to break. (D) Stress to break. Light-shaded markers represent actual measurements, dark-shaded markers represent averages, and error bars indicate 95% CI.

Photorheology. Beyond yield stress, hydrogel inks change their structure from a "solid-like" to a "liquid-like" state (**Error! Reference source not found.**-4). While printing, the weight of the upper layers exert stress, which can cause the printed object to collapse, thereby limiting the height

of printed objects. For example, ink with 2.4% CNC, deforms at 50 Pa and, therefore, the maximal achievable height would be 0.5 cm, assuming $\rho = 1000 \frac{kg}{m^3}$.[12] In practice, the height will be even lower due to the impact of capillary forces. To overcome the height limitation, it is necessary to polymerize the hydrogel before the printing process reaches its yield-stress-dictated height limitation. Photorheology experiments provide a good tool to detect the transition from a "liquid-like" to a "solid-like" state via photopolymerization. Therefore, UV photopolymerization was induced to rapidly introduce covalent and permanent crosslinks in the hydrogel, which increases ink rheology temporary fixation yield stress and can withstand the addition of more printed layers.

Based on the observed rheological and mechanical properties, the ink containing 2.4% CNC was selected for photorheological assessment. The photorheology measurements showed that this ink achieves sufficient viscosity that enabled structure fixation within several seconds, and required approximately 20 s of irradiation to obtain a fully polymerized hydrogel (**Figure** 7). It should be noted that the same final viscosity was observed for CNC-free ink, its initial viscosity was too low for printing by DIW.

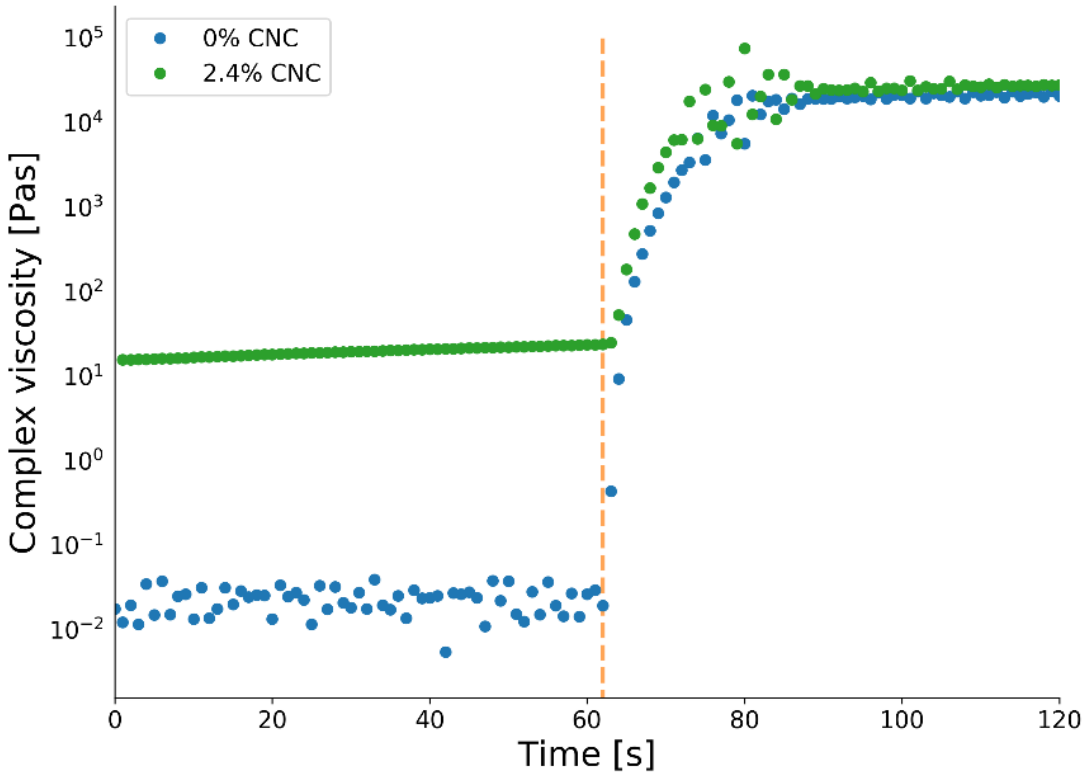

Figure 7. Photorheology characterization of water-soluble PI photopolymerization kinetics for 0 and 2.4 % CNC inks. Vertical dashed line indicate the time point at which the light was turned on.

3D Printing. To demonstrate the importance of rapid UV curing, 2.4% CNC ink was UV-irradiated during printing or after the entire object was printed (Figure S5-6). Figure 8A shows printed cylinders subjected to UV irradiation (5 s) after each layer was printed. A gradual increase in height with a good fixation of the cylinder was achieved, with no seeing limitation to the final object height. In contrast, when UV irradiation was only applied after the entire cylinder was printed, the lower part (from layer #4 and on) of the cylinder expanded, indicating the collapse of the object (Figure 8B). When reaching layer #14, the supposed-to-be cylinder object slumped and the printing had to be terminated.

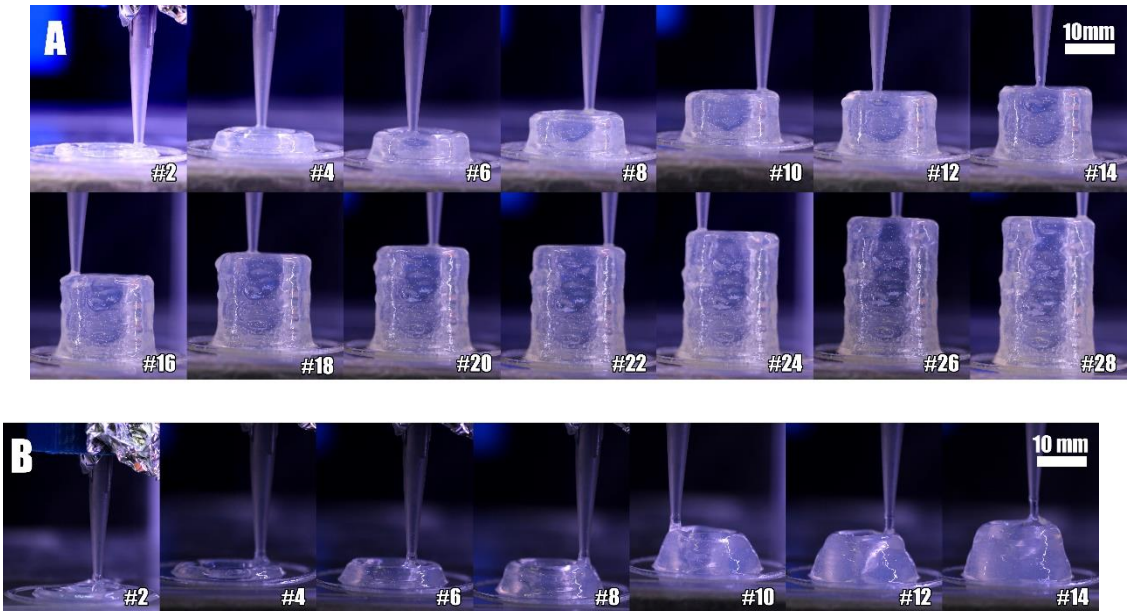

Figure 8. 2.4% CNC DIW-printed cylindrical objects photographed at two-layer intervals during the printing process, with rapid UV curing performed (A) after deposition of each layer or (B) after the entire object was printed. The printed layers are indicated at the bottom of each image.

The cylinders presented in Figure 8 were printed with a 1.29 mm nozzle diameter, to achieve large heights in a short time. The same inks can be printed using much smaller nozzle diameters, which provide enhanced resolution. Figure S8 shows a series of lines printed using the same ink, but through a series of nozzles of decreasing diameters.

These experiments were performed using 365 nm UV light, which might be problematic for biomedical applications, due to the negative effect of short-wavelength radiation on cell viability. To test the curating effectiveness of visible light, these same printing experiments were repeated with 405 nm irradiation. As shown in Figure S7 and Figure 9A, the same degree of fixation was achieved, without compromising the printing speed or resolution.

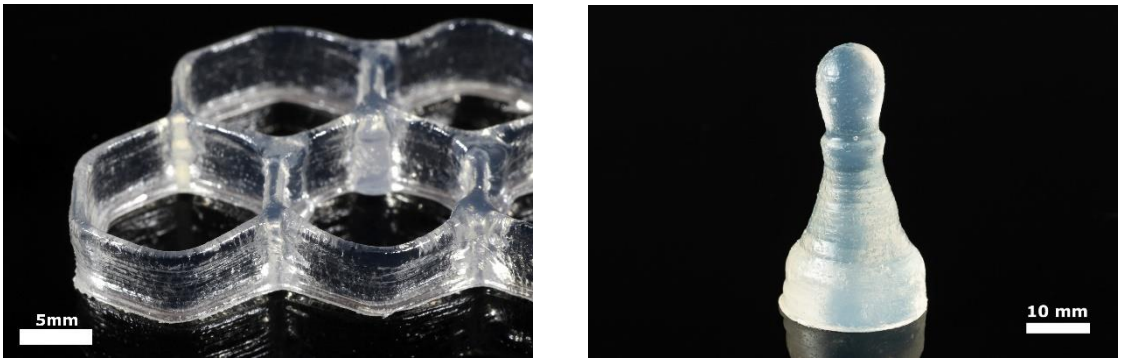

(A) (B)

Figure 9. DIW hydrogel structures printed with rapid photopolymerization. (A) A honeycomb-shaped object cured with 405nm irradiation. (B) A chess pawn cured with 365nm light.

CONCLUSIONS

Acrylic acid-based hydrogels reinforced with CNC were 3D printed and photopolymerized by using a water-compatible PI. The CNC imparted a unique rheological behavior, which manifested by orders of magnitude different behaviors at low versus high shear rates, and fast and high shear recovery, without compromising ink printability. Rapid photopolymerization performed immediately after printing each layer overcame the common height limit of DIW printing of hydrogels, and enabled the fabrication of objects with a high-aspect ratio. The presented approach enabled the shortest irradiation time under extremely low concentrations of PI, including possible curing by 405 nm light, which is important for maintaining viability in bio-inks.

ASSOCIATED CONTENT

Supporting Information.

The following files are available free of charge.

brief description (file type, i.e., PDF)

AUTHOR INFORMATION

Corresponding Author

*Oded Shoseyov: shoseyov@agri.huji.ac.il

*Shlomo Magdassi: magdassi@mail.huji.ac.il

Author Contributions

The manuscript was written through contributions of all authors. All authors have given approval to the final version of the manuscript.

Funding Sources

We thank the Ministry of Science Technology and Space in Israel for financial support (3-15638).

ACKNOWLEDGMENT

The authors would like to thank Prof. Morton M. Denn for fruitful discussions on rheology.

ABBREVIATIONS

DIW, direct ink writing; CNC, cellulose nanocrystals; PI, photoinitiator; PDMA, poly(N,N-dimethacrylamide); LAP, lithium phenyl-2,4,6-trimethylbenzoylphosphinate; AA, Acrylic acid; IPA, isopropanol; TPO, 2,4,6-trimethylbenzoyl-diphenylphosphine oxide; CI, confidence interval; PEGDA, Polyethyleneglycol diacrylate.

REFERENCES

(1) Martin, J. H.; Yahata, B. D.; Hundley, J. M.; Mayer, J. A.; Schaedler, T. A.; Pollock, T. M. 3D Printing of High-Strength Aluminium Alloys. *Nature* **2017**, *549* (7672), 365–369. https://doi.org/10.1038/nature23894.

(2) Tepylo, N.; Huang, X.; Patnaik, P. C. Laser-Based Additive Manufacturing Technologies for Aerospace Applications. *Adv. Eng. Mater.* **2019**, *21* (11), 1–35. https://doi.org/10.1002/adem.201900617.

(3) Dawood, A.; Marti, B. M.; Sauret-Jackson, V.; Darwood, A. 3D Printing in Dentistry. *Br. Dent. J.* **2015**, *219* (11), 521–529. https://doi.org/10.1038/sj.bdj.2015.914.

(4) Sachyani Keneth, E.; Kamyshny, A.; Totaro, M.; Beccai, L.; Magdassi, S. 3D Printing Materials for Soft Robotics. *Adv. Mater.* **2020**, *2003387*, 1–17. https://doi.org/10.1002/adma.202003387.

(5) Mathew, E.; Pitzanti, G.; Larrañeta, E.; Lamprou, D. A. Three-Dimensional Printing of Pharmaceuticals and Drug Delivery Devices. *Pharmaceutics* **2020**, *12* (3), 1–9. https://doi.org/10.3390/pharmaceutics12030266.

(6) Noor, N.; Shapira, A.; Edri, R.; Gal, I.; Wertheim, L.; Dvir, T. 3D Printing of Personalized Thick and Perfusable Cardiac Patches and Hearts. *Adv. Sci.* **2019**, *6* (11). https://doi.org/10.1002/advs.201900344.

(7) Jammalamadaka, U.; Tappa, K. Recent Advances in Biomaterials for 3D Printing and Tissue Engineering. *J. Funct. Biomater.* **2018**, *9* (1). https://doi.org/10.3390/jfb9010022.

(8) Dong, Y.; Wang, S.; Ke, Y.; Ding, L.; Zeng, X.; Magdassi, S.; Long, Y. 4D Printed Hydrogels: Fabrication, Materials, and Applications. *Adv. Mater. Technol.* **2020**, *5* (6), 1–

19. https://doi.org/10.1002/admt.202000034.

(9) Ge, Q.; Chen, Z.; Cheng, J.; Zhang, B.; Zhang, Y.; Li, H. 3D Printing of Highly Stretchable Hydrogel with Diverse UV Curable Polymers. **2021**, 1–11.

(10) Cui, X.; Breitenkamp, K.; Finn, M. G.; Lotz, M.; D'Lima, D. D. Direct Human Cartilage Repair Using Three-Dimensional Bioprinting Technology. *Tissue Eng. - Part A* **2012**, *18* (11–12), 1304–1312. https://doi.org/10.1089/ten.tea.2011.0543.

(11) Fonseca, A. C.; Melchels, F. P. W.; Ferreira, M. J. S.; Moxon, S. R.; Potjewyd, G.; Dargaville, T. R.; Kimber, S. J.; Domingos, M. Emulating Human Tissues and Organs: A Bioprinting Perspective Toward Personalized Medicine. *Chem. Rev.* **2020**, *120* (19), 11128–11174. https://doi.org/10.1021/acs.chemrev.0c00342.

(12) M'Barki, A.; Bocquet, L.; Stevenson, A. Linking Rheology and Printability for Dense and Strong Ceramics by Direct Ink Writing. *Sci. Rep.* **2017**, *7* (1), 1–10. https://doi.org/10.1038/s41598-017-06115-0.

(13) Napadensky, E. Inkjet 3D Printing. In *The Chemistry of Inkjet Inks*; Magdassi, S., Ed.; 2009; pp 255–268. https://doi.org/10.1142/9789812818225_0013.

(14) Mora-Boza, A.; Włodarczyk-Biegun, M. K.; Del Campo, A.; Vázquez-Lasa, B.; Román, J. S. Glycerylphytate as an Ionic Crosslinker for 3D Printing of Multi-Layered Scaffolds with Improved Shape Fidelity and Biological Features. *Biomater. Sci.* **2020**, *8* (1), 506–516. https://doi.org/10.1039/c9bm01271k.

(15) Zhuang, P.; Ng, W. L.; An, J.; Chua, C. K.; Tan, L. P. Layer-by-Layer Ultraviolet Assisted Extrusion-Based (UAE) Bioprinting of Hydrogel Constructs with High Aspect Ratio for

Soft Tissue Engineering Applications. *PLoS One* **2019**, *14* (6), 1–21. https://doi.org/10.1371/journal.pone.0216776.

(16) Pawar, A. A.; Saada, G.; Cooperstein, I.; Larush, L.; Jackman, J. A.; Tabaei, S. R.; Cho, N.-J. J.; Magdassi, S. High-Performance 3D Printing of Hydrogels by Water-Dispersible Photoinitiator Nanoparticles. *Sci. Adv.* **2016**, *2* (4), 1–8. https://doi.org/10.1126/sciadv.1501381.

(17) Kam, D.; Layani, M.; BarkaiMinerbi, S.; Orbaum, D.; Abrahami BenHarush, S.; Shoseyov, O.; Magdassi, S. Additive Manufacturing of 3D Structures Composed of Wood Materials. *Adv. Mater. Technol.* **2019**, *1900158* (9), 1900158. https://doi.org/10.1002/admt.201900158.

(18) Kam, D.; Chasnitsky, M.; Nowogrodski, C.; Braslavsky, I.; Abitbol, T.; Magdassi, S.; Shoseyov, O. Direct Cryo Writing of Aerogels Via 3D Printing of Aligned Cellulose Nanocrystals Inspired by the Plant Cell Wall. *Colloids and Interfaces* **2019**, *3* (2), 46. https://doi.org/10.3390/colloids3020046.

(19) Beck-Candanedo, S.; Roman, M.; Gray, D. G. Effect of Reaction Conditions on the Properties and Behavior of Wood Cellulose Nanocrystal Suspensions. *Biomacromolecules* **2005**, *6* (2), 1048–1054. https://doi.org/10.1021/bm049300p.

(20) Abitbol, T.; Kam, D.; Levi-Kalisman, Y.; Gray, D. G.; Shoseyov, O. Surface Charge Influence on the Phase Separation and Viscosity of Cellulose Nanocrystals. *Langmuir* **2018**, *34* (13), 3925–3933. https://doi.org/10.1021/acs.langmuir.7b04127.

(21) De France, K. J.; Hoare, T.; Cranston, E. D. Review of Hydrogels and Aerogels Containing

Nanocellulose. *Chem. Mater.* **2017**, *29* (11), 4609–4631. https://doi.org/10.1021/acs.chemmater.7b00531.

(22) Wang, J.; Siqueira, G.; Müller, G.; Rentsch, D.; Huch, A.; Tingaut, P.; Levalois-Grützmacher, J.; Grützmacher, H. Synthesis of New Bis(Acyl)Phosphane Oxide Photoinitiators for the Surface Functionalization of Cellulose Nanocrystals. *Chem. Commun.* **2016**, *52* (13), 2823–2826. https://doi.org/10.1039/c5cc09760f.

(23) Siqueira, G.; Kokkinis, D.; Libanori, R.; Hausmann, M. K.; Gladman, A. S.; Neels, A.; Tingaut, P.; Zimmermann, T.; Lewis, J. A.; Studart, A. R. Cellulose Nanocrystal Inks for 3D Printing of Textured Cellular Architectures. *Adv. Funct. Mater.* **2017**, *27* (12), 1604619. https://doi.org/10.1002/adfm.201604619.

(24) Yang, J.; Han, C. R.; Xu, F.; Sun, R. C. Simple Approach to Reinforce Hydrogels with Cellulose Nanocrystals. *Nanoscale* **2014**, *6* (11), 5934–5943. https://doi.org/10.1039/c4nr01214c.

(25) Kelly, J. A.; Shukaliak, A. M.; Cheung, C. C. Y.; Shopsowitz, K. E.; Hamad, W. Y.; MacLachlan, M. J. Responsive Photonic Hydrogels Based on Nanocrystalline Cellulose. *Angew. Chemie - Int. Ed.* **2013**, *52* (34), 8912–8916. https://doi.org/10.1002/anie.201302687.

(26) Wang, P. X.; Hamad, W. Y.; MacLachlan, M. J. Structure and Transformation of Tactoids in Cellulose Nanocrystal Suspensions. *Nat. Commun.* **2016**, *7*. https://doi.org/10.1038/ncomms11515.

(27) Zhang, Z.; Liu, R.; Zepeda, H.; Zeng, L.; Qiu, J.; Wang, S. 3D Printing Super Strong

Hydrogel for Artificial Meniscus. *ACS Appl. Polym. Mater.* **2019**, *1* (8), 2023–2032. https://doi.org/10.1021/acsapm.9b00304.

(28) Frost, B.; Sutliff, B. P.; Thayer, P.; Bortner, M. J.; Foster, E. J. Gradient Poly(Ethylene Glycol) Diacrylate and Cellulose Nanocrystals Tissue Engineering Composite Scaffolds via Extrusion Bioprinting. *Front. Bioeng. Biotechnol.* **2019**, *7* (OCT), 1–14. https://doi.org/10.3389/fbioe.2019.00280.

(29) Li, V. C. F.; Kuang, X.; Mulyadi, A.; Hamel, C. M.; Deng, Y.; Qi, H. J. 3D Printed Cellulose Nanocrystal Composites through Digital Light Processing. *Cellulose* **2019**, *26* (6), 3973–3985. https://doi.org/10.1007/s10570-019-02353-9.

(30) Palaganas, N. B.; Mangadlao, J. D.; De Leon, A. C. C.; Palaganas, J. O.; Pangilinan, K. D.; Lee, Y. J.; Advincula, R. C. 3D Printing of Photocurable Cellulose Nanocrystal Composite for Fabrication of Complex Architectures via Stereolithography. *ACS Appl. Mater. Interfaces* **2017**, *9* (39), 34314–34324. https://doi.org/10.1021/acsami.7b09223.

(31) Wang, J.; Chiappone, A.; Roppolo, I.; Shao, F.; Fantino, E.; Lorusso, M.; Rentsch, D.; Dietliker, K.; Pirri, C. F.; Grützmacher, H. All-in-One Cellulose Nanocrystals for 3D Printing of Nanocomposite Hydrogels. *Angew. Chemie - Int. Ed.* **2018**, *57* (9), 2353–2356. https://doi.org/10.1002/anie.201710951.

(32) Ding, H.; Illsley, N. P.; Chang, R. C. 3D Bioprinted GelMA Based Models for the Study of Trophoblast Cell Invasion. *Sci. Rep.* **2019**, *9* (1), 1–13. https://doi.org/10.1038/s41598-019-55052-7.

(33) Lai, C. W.; Yu, S. S. 3D Printable Strain Sensors from Deep Eutectic Solvents and Cellulose

Nanocrystals. *ACS Appl. Mater. Interfaces* **2020**, *12* (30), 34235–34244. https://doi.org/10.1021/acsami.0c11152.

(34) Wei, J.; Wang, J.; Su, S.; Wang, S.; Qiu, J.; Zhang, Z.; Christopher, G.; Ning, F.; Cong, W. 3D Printing of an Extremely Tough Hydrogel. *RSC Adv.* **2015**, *5* (99), 81324–81329. https://doi.org/10.1039/c5ra16362e.

(35) Huang, T. Q.; Qu, X.; Liu, J.; Chen, S. 3D Printing of Biomimetic Microstructures for Cancer Cell Migration. *Biomed. Microdevices* **2014**, *16* (1), 127–132. https://doi.org/10.1007/s10544-013-9812-6.

(36) Yeh, Y. C.; Highley, C. B.; Ouyang, L.; Burdick, J. A. 3D Printing of Photocurable Poly(Glycerol Sebacate) Elastomers. *Biofabrication* **2016**, *8* (4). https://doi.org/10.1088/1758-5090/8/4/045004.

(37) Larush, L.; Kaner, I.; Fluksman, A.; Tamsut, A.; Pawar, A. A.; Lesnovski, P.; Benny, O.; Magdassi, S. 3D Printing of Responsive Hydrogels for Drug-Delivery Systems. *J. 3D Print. Med.* **2017**, *1* (4), 219–229. https://doi.org/10.2217/3dp-2017-0009.

(38) Ouyang, L.; Highley, C. B.; Rodell, C. B.; Sun, W.; Burdick, J. A. 3D Printing of Shear-Thinning Hyaluronic Acid Hydrogels with Secondary Cross-Linking. *ACS Biomater. Sci. Eng.* **2016**, *2* (10), 1743–1751. https://doi.org/10.1021/acsbiomaterials.6b00158.

(39) Fantino, E.; Roppolo, I.; Zhang, D.; Xiao, J.; Chiappone, A.; Castellino, M.; Guo, Q.; Pirri, C. F.; Yang, J. 3D Printing/Interfacial Polymerization Coupling for the Fabrication of Conductive Hydrogel. *Macromol. Mater. Eng.* **2018**, *303* (4), 1–8. https://doi.org/10.1002/mame.201700356.

(40) Murphy, R. D.; Kimmins, S.; Hibbitts, A. J.; Heise, A. 3D-Extrusion Printing of Stable Constructs Composed of Photoresponsive Polypeptide Hydrogels. *Polym. Chem.* **2019**, *10* (34), 4675–4682. https://doi.org/10.1039/c9py00796b.

(41) Smith, P. T.; Narupai, B.; Tsui, J. H.; Millik, S. C.; Shafranek, R. T.; Kim, D. H.; Nelson, A. Additive Manufacturing of Bovine Serum Albumin-Based Hydrogels and Bioplastics. *Biomacromolecules* **2020**, *21* (2), 484–492. https://doi.org/10.1021/acs.biomac.9b01236.

(42) Kiyotake, E. A.; Douglas, A. W.; Thomas, E. E.; Nimmo, S. L.; Detamore, M. S. Development and Quantitative Characterization of the Precursor Rheology of Hyaluronic Acid Hydrogels for Bioprinting. *Acta Biomater.* **2019**, *95*, 176–187. https://doi.org/10.1016/j.actbio.2019.01.041.

(43) Heo, D. N.; Lee, S. J.; Timsina, R.; Qiu, X.; Castro, N. J.; Zhang, L. G. Development of 3D Printable Conductive Hydrogel with Crystallized PEDOT:PSS for Neural Tissue Engineering. *Mater. Sci. Eng. C* **2019**, *99* (September 2018), 582–590. https://doi.org/10.1016/j.msec.2019.02.008.

(44) Hong, H.; Seo, Y. B.; Kim, D. Y.; Lee, J. S.; Lee, Y. J.; Lee, H.; Ajiteru, O.; Sultan, M. T.; Lee, O. J.; Kim, S. H.; Park, C. H. Digital Light Processing 3D Printed Silk Fibroin Hydrogel for Cartilage Tissue Engineering. *Biomaterials* **2020**, *232* (November 2019), 119679. https://doi.org/10.1016/j.biomaterials.2019.119679.

(45) Xue, D.; Zhang, J.; Wang, Y.; Mei, D. Digital Light Processing-Based 3D Printing of Cell-Seeding Hydrogel Scaffolds with Regionally Varied Stiffness. *ACS Biomater. Sci. Eng.* **2019**, *5* (9), 4825–4833. https://doi.org/10.1021/acsbiomaterials.9b00696.

(46) Grogan, S. P.; Chung, P. H.; Soman, P.; Chen, P.; Lotz, M. K.; Chen, S.; D'Lima, D. D. Digital Micromirror Device Projection Printing System for Meniscus Tissue Engineering. *Acta Biomater.* **2013**, *9* (7), 7218–7226. https://doi.org/10.1016/j.actbio.2013.03.020.

(47) Highley, C. B.; Rodell, C. B.; Burdick, J. A. Direct 3D Printing of Shear-Thinning Hydrogels into Self-Healing Hydrogels. *Adv. Mater.* **2015**, *27* (34), 5075–5079. https://doi.org/10.1002/adma.201501234.

(48) Melilli, G.; Carmagnola, I.; Tonda-Turo, C.; Pirri, F.; Ciardelli, G.; Sangermano, M.; Hakkarainen, M.; Chiappone, A. DLP 3D Printing Meets Lignocellulosic Biopolymers: Carboxymethyl Cellulose Inks for 3D Biocompatible Hydrogels. *Polymers (Basel).* **2020**, *12* (8), 1–11. https://doi.org/10.3390/POLYM12081655.

(49) Shen, Y.; Tang, H.; Huang, X.; Hang, R.; Zhang, X.; Wang, Y.; Yao, X. DLP Printing Photocurable Chitosan to Build Bio-Constructs for Tissue Engineering. *Carbohydr. Polym.* **2020**, *235* (October 2019), 115970. https://doi.org/10.1016/j.carbpol.2020.115970.

(50) Basara, G.; Yue, X.; Zorlutuna, P. Dual Crosslinked Gelatin Methacryloyl Hydrogels For. **2019**.

(51) Burke, G.; Devine, D. M.; Major, I. Effect of Stereolithography 3d Printing on the Properties of Pegdma Hydrogels. *Polymers (Basel).* **2020**, *12* (9), 1–13. https://doi.org/10.3390/polym12092015.

(52) Tytgat, L.; Van Damme, L.; Ortega Arevalo, M. del P.; Declercq, H.; Thienpont, H.; Otteveare, H.; Blondeel, P.; Dubruel, P.; Van Vlierberghe, S. Extrusion-Based 3D Printing of Photo-Crosslinkable Gelatin and κ-Carrageenan Hydrogel Blends for Adipose Tissue

Regeneration. *Int. J. Biol. Macromol.* **2019**, *140*, 929–938. https://doi.org/10.1016/j.ijbiomac.2019.08.124.

(53) Li, L.; Lu, C.; Wang, L.; Chen, M.; White, J.; Hao, X.; McLean, K. M.; Chen, H.; Hughes, T. C. Gelatin-Based Photocurable Hydrogels for Corneal Wound Repair. *ACS Appl. Mater. Interfaces* **2018**, *10* (16), 13283–13292. https://doi.org/10.1021/acsami.7b17054.

(54) Pawar, A. A.; Saada, G.; Cooperstein, I.; Larush, L.; Jackman, J. A.; Tabaei, S. R.; Cho, N.-J. J.; Magdassi, S. High-Performance 3D Printing of Hydrogels by Water-Dispersible Photoinitiator Nanoparticles. *Sci. Adv.* **2016**, *2* (4), 1–8. https://doi.org/10.1126/sciadv.1501381.

(55) Hiller, A.; Borchers, K.; Tovar, G. E. M.; Southan, A. Impact of Intermediate UV Curing and Yield Stress of 3D Printed Poly(Ethylene Glycol) Diacrylate Hydrogels on Interlayer Connectivity and Maximum Build Height. *Addit. Manuf.* **2017**, *18*, 136–144. https://doi.org/10.1016/j.addma.2017.10.008.

(56) Jeon, O.; Lee, Y. Bin; Jeong, H.; Lee, S. J.; Wells, D.; Alsberg, E. Individual Cell-Only Bioink and Photocurable Supporting Medium for 3D Printing and Generation of Engineered Tissues with Complex Geometries. *Mater. Horizons* **2019**, *6* (8), 1625–1631. https://doi.org/10.1039/c9mh00375d.

(57) Xia, H.; Zhao, D.; Zhu, H.; Hua, Y.; Xiao, K.; Xu, Y.; Liu, Y.; Chen, W.; Liu, Y.; Zhang, W.; Liu, W.; Tang, S.; Cao, Y.; Wang, X.; Chen, H. H.; Zhou, G. Lyophilized Scaffolds Fabricated from 3D-Printed Photocurable Natural Hydrogel for Cartilage Regeneration. *ACS Appl. Mater. Interfaces* **2018**, *10* (37), 31704–31715. https://doi.org/10.1021/acsami.8b10926.

(58) Müller, L. A. E.; Zimmermann, T.; Nyström, G.; Burgert, I.; Siqueira, G. Mechanical Properties Tailoring of 3D Printed Photoresponsive Nanocellulose Composites. *Adv. Funct. Mater.* **2020**, *2002914*, 2002914. https://doi.org/10.1002/adfm.202002914.

(59) Johnston, T. G.; Fellin, C. R.; Carignano, A.; Nelson, A. Poly(Alkyl Glycidyl Ether) Hydrogels for Harnessing the Bioactivity of Engineered Microbes. *Faraday Discuss.* **2019**, *219*, 58–72. https://doi.org/10.1039/c9fd00019d.

(60) Yin, M. J.; Yao, M.; Gao, S.; Zhang, A. P.; Tam, H. Y.; Wai, P. K. A. Rapid 3D Patterning of Poly(Acrylic Acid) Ionic Hydrogel for Miniature PH Sensors. *Adv. Mater.* **2016**, *28* (7), 1394–1399. https://doi.org/10.1002/adma.201504021.

(61) Wang, Y.; Li, Y.; Yu, X.; Long, Q.; Zhang, T. Synthesis of a Photocurable Acrylated Poly(Ethylene Glycol)-: Co -Poly(Xylitol Sebacate) Copolymers Hydrogel 3D Printing Ink for Tissue Engineering. *RSC Adv.* **2019**, *9* (32), 18394–18405. https://doi.org/10.1039/c9ra03637g.

(62) Wang, L. L.; Highley, C. B.; Yeh, Y. C.; Galarraga, J. H.; Uman, S.; Burdick, J. A. Three-Dimensional Extrusion Bioprinting of Single- and Double-Network Hydrogels Containing Dynamic Covalent Crosslinks. *J. Biomed. Mater. Res. - Part A* **2018**, *106* (4), 865–875. https://doi.org/10.1002/jbm.a.36323.

(63) Wilts, E. M.; Pekkanen, A. M.; White, B. T.; Meenakshisundaram, V.; Aduba, D. C.; Williams, C. B.; Long, T. E. Vat Photopolymerization of Charged Monomers: 3D Printing with Supramolecular Interactions. *Polym. Chem.* **2019**, *10* (12), 1442–1451. https://doi.org/10.1039/c8py01792a.